

# Internal Feedback in Biological Control: Locality and System Level Synthesis

Jing Shuang (Lisa) Li

**Abstract**—The presence of internal feedback pathways (IFPs) is an ubiquitous yet unexplained phenomenon in the brain. Motivated by experimental observations on 1) motor-related signals in visual areas, and 2) massively distributed processing in the brain, we approach this problem from a sensorimotor standpoint and make use of distributed optimal controllers to explain IFPs. We use the System Level Synthesis (SLS) controller to model neuronal phenomena such as signaling delay, local processing, and local reaction. Based on the SLS controller, we make qualitative theoretical predictions about IFPs that has strong alignment with experimental and imaging studies. In particular, we introduce a necessary ‘mesocircuit’ for optimal performance with distributed and local processing, and local disturbance rejection; this ‘mesocircuit’ requires extreme amounts of IFPs and memory for proper function. This is the first theory that can replicate the massive amounts of IFPs in the brain purely from *a priori* principles, providing a new and promising theoretical basis upon which we can build to better understand the inner workings of the brain.

## I. INTRODUCTION

The primate visual cortex entails connections that propagate information from the retina in the eye to the lateral geniculate nucleus (LGN), then to the primary visual area (V1) in the cortex, secondary visual area (V2), and so on. However, massive amounts of connections in the reverse direction (i.e. internal feedback pathways, or IFP) are also observed, as shown in the left panel of Fig. 1. These connections are known by a variety of names in the neuroscientific literature, including *descending feedback*, *predictive feedback*, *reciprocal connections*, and *recurrence*. Feedback is a well-documented but poorly understood architectural feature [3]–[5], and understanding the purpose of the mechanism is invaluable to understanding overall circuit function in the visual system.

Motivated by recent findings showing that non-visual-related neuronal activity in the visual areas – which are substantial and thus far unexplained – are dominated by body movements [7], [8], we propose to view IFPs from a sensorimotor perspective. Optimal control models are an ideal candidate for this analysis as they have been widely successful in explaining behavior-level observations in the sensorimotor domain [9], [10]. A desirable next step is to use optimal control to unravel the mysteries of the *architecture* and structural function of the sensorimotor system. However, this presents a major challenge: the underlying components

(e.g. cells, neurons) of biological systems are vastly different from the underlying components (e.g. electrical wires, chips) used to implement man-made optimal controllers. Generally speaking, man-made controllers use fast electronic parts, which are relatively ideal; comparatively, biological controllers use cells and neurons as parts, which are much more constrained. Some key differences are listed in Table I. Although these are only a subset of ideal vs. constrained conditions, we will show that this particular subset of constraints allows us to make substantial *a priori* predictions about biological systems.

TABLE I  
IDEAL VS. CONSTRAINED CONTROLLER COMPONENTS

	Communication	Actuation & Sensing
Ideal	dense, fast, global	dense, fast
Constrained	sparse, delayed, local	sparse, delayed

In our companion paper [2], we model basic actuation and sensing delay using a slight variation of standard optimal control, and demonstrate that IFPs are required for optimal function when delays (from sensor to controller, or controller to actuation) are present. However, standard optimal control cannot capture local, distributed, and delayed communication *within the controller* – this requires the newer System Level Synthesis (SLS) theory [11]. In this paper, we use an SLS controller to capture local, distributed, and delayed communication, and show that it not only motivates the presence of IFPs, but motivates extreme amounts of IFPs that match neural anatomy [6]. In Section II, we discuss the effect of sparse closed-loops and sparse controllers, and use an intermediate parametrization to introduce the notion of local memory patches. We then leverage these concepts in Section III to describe the full SLS-based mesocircuit, and examine the massive amounts of IFPs that are intrinsic to this mesocircuit. Section IV contains closing remarks. For more thorough motivation from a biology/neuroscience perspective, we refer the reader to our companion paper [1].

The focus of this work is to provide standalone theory, which can inform us of fruitful experimental directions and guide interpretations of large-scale, high-dimensional data. Though we do not include empirical data from here, we discuss possible experiments and biological systems of interest in [1].

IFPs are by no means a phenomenon unique to the visual system; they are prevalent across neural systems, and has been observed in the somatosensory and motor cortices [3],

J. S. Li is with Computing and Mathematical Sciences, California Institute of Technology. [jsli@caltech.edu](mailto:jsli@caltech.edu). This research was in part supported by NSERC PGSD3-557385-2021

This paper is one of three in a series on internal feedback in biological control architectures. These papers may be read in any order, though a suggested order is [1], [2], then this paper.

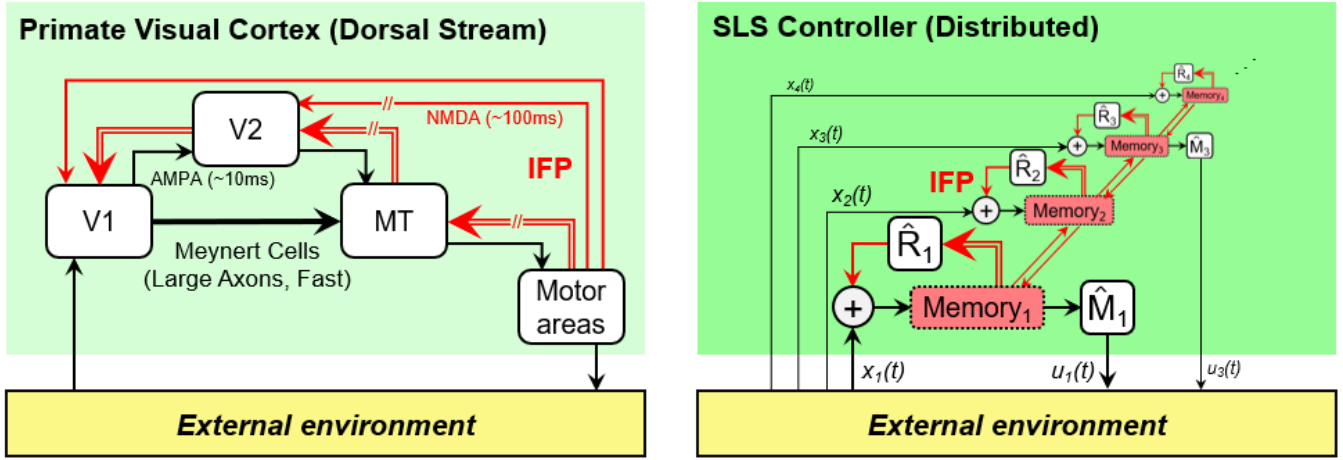


Fig. 1. Forward pathways are shown in black; internal feedback pathways (IFPs) are shown in red. The forward direction travels from sensing toward actuation (left to right); internal feedback travels from actuation back toward sensing (right to left). Compound-line arrows indicate larger signals/multiple connections (e.g. vectors instead of scalars). (Left) Primate visual cortex demonstrates existence of large amounts of IFPs, often outnumbering the forward paths [6]. Not shown is the massively distributed processing that also occurs in primate visual cortex and everywhere in the brain. (Right) System Level Synthesis (SLS) controller with localized processing and memory, displaying large amounts of IFPs. The localized processing feature alone motivates an explosion in the number of IFPs, which matches experimental observations in primate cortex. [3], [6]

auditory system [12], and other structures in the brain, as well as cellular systems. Though our work focuses on the sensorimotor system, the subsequent analysis is sufficiently general to be of potential use in other domains as well. Additionally, an understanding of IFPs is highly beneficial for the design of modern infrastructure (e.g. smart grids). Although fast electronic parts generally allow engineers to avoid the constraints listed in Table I, such constraints become unavoidable as we move toward efficient, sustainable, large networked systems. An understanding of the role of IFPs in architectures with constrained components enables engineers to fully exploit the full range of engineering components to create the best possible performance for future systems.

## II. CLOSED LOOPS, SPARSITY, AND MEMORY

We focus on the state feedback problem; all our results also apply to its dual, the full control problem. We focus on sparse (e.g. local) and distributed processing in the controller, and also sparse and local reactions in the closed-loop. Though there are many different mechanisms (e.g. delay, internal estimation, as per [2]) that necessitate IFPs, sparse processing in the controller appears to be the single mechanism that predicts the biggest explosion of IFPs. By observing such mechanisms one at a time, we are able to produce simple, human-interpretable models that we will eventually combine to create more complete (albeit indecipherably complex, like the brain) and quantitative models.

### A. Closed Loops and Sparsity

Consider the linear time-invariant discrete-time system described in frequency domain by

$$z\mathbf{x} = A\mathbf{x} + B\mathbf{u} + \mathbf{w} \quad (1)$$

where  $\mathbf{x}$ ,  $\mathbf{u}$ , and  $\mathbf{w}$  denote state, input, and disturbance, respectively. Assume we sense the state. We apply a linear

transfer matrix  $\mathbf{K}$  as the controller, i.e.  $\mathbf{u} = \mathbf{K}\mathbf{x}$ , and define the resulting closed-loop responses  $\mathbf{R}, \mathbf{M}$  as in [11]:

$$\begin{bmatrix} \mathbf{x} \\ \mathbf{u} \end{bmatrix} = \begin{bmatrix} \mathbf{R} \\ \mathbf{M} \end{bmatrix} \mathbf{w} \quad (2)$$

which are related to  $\mathbf{K}$  through

$$\mathbf{R} = (zI - A - B\mathbf{K})^{-1}, \quad \mathbf{M} = \mathbf{K}\mathbf{R} \quad (3)$$

We can write out  $\mathbf{M}$  as the sum of spectral components  $M(k)$

$$\mathbf{M} = \sum_{k=0}^{\infty} M(k)z^{-k} \quad (4)$$

Suppose we have  $\mathbf{u} = \mathbf{M}\mathbf{w}$ , and the system is perturbed by an impulse at node  $i$ , time  $t$ . Then, the impulse response from time  $t$  to  $t+k$ , i.e.  $u(t:t+k)$ , can be obtained by looking at the  $i$ th column of  $M(0), M(1) \dots M(k)$ . We can similarly write  $\mathbf{R}$  and  $\mathbf{K}$  in terms of spectral components, though  $\mathbf{K}$  is often a static matrix; for LQR, we solve for a static gain  $K_{LQR}$  and set  $K(0) = K_{LQR}$  and  $K(k) = 0 \forall i > 0$ . As in [11], we constrain  $\mathbf{R}$  and  $\mathbf{M}$  to be stable and strictly causal, i.e.  $M(0) = 0$ . For simplicity, we will work with finite-horizon  $\mathbf{R}, \mathbf{M}$ .

Typically, we design  $\mathbf{K}$  and implement it on the system. We want  $\mathbf{K}$ , in conjunction with the plant, to give a closed-loop system that achieves some desired performance. In large systems, we may also want some sparsity in the controller  $\mathbf{K}$  and closed-loop responses  $\mathbf{R}$  and  $\mathbf{M}$ . We will focus on local communication and local reaction as the two main sources of sparsity constraints; both are abundant in biological and nervous systems.

1) *Local communication*: Neurons communicate locally – each neuron typically communicates only with a handful of nearby neurons, which comprise a very tiny subset of the organism’s total neurons. Local communication imposes

local sparsity structure on the controller; in the standard case,  $\mathbf{K}$ . Local communication is desirable in large cyberphysical systems such as the smart grid, in which centralized communication and coordination is unwieldy.

2) *Local disturbance rejection*: Biological systems react locally; reflexes are often used to contain and reject disturbances using only local actuators, without affecting the entire organism. Local reaction imposes local sparsity structure on the closed-loop responses  $\mathbf{R}$  and  $\mathbf{M}$ . Local reaction is desirable in systems such as the smart grid, where we do not want a disturbance at one part of the grid to propagate throughout the entire grid.

In an ideal system (refer to Table I), we obtain sparsity for free, i.e. without specifying it as a constraint or objective. For an LQR problem with no input penalty, the optimal controller  $K$  has the same sparsity as the state matrix  $A$ , and gives rise to similarly sparse deadbeat closed-loop responses  $\mathbf{R}$ ,  $\mathbf{M}$ . In our system,  $A$  is extremely sparse and local (i.e. nodes only affect their neighbors); thus, the resulting optimal controller and closed-loop responses are sparse and local. However, in a non-ideal system (e.g. sparse actuation instead of full actuation), we no longer obtain this desired sparsity.

To demonstrate, we use a symmetric 8-node ring, shown in the top left of Fig. 5. The state matrix  $A \in \mathbb{R}^{8 \times 8}$  is

$$A = \frac{a}{3} * \begin{bmatrix} 1 & 1 & 0 & \dots & 1 \\ 1 & 1 & 1 & 0 & \dots \\ 0 & \ddots & \ddots & \ddots & \vdots \\ \vdots & \ddots & \ddots & \ddots & 1 \\ 1 & 0 & \dots & 1 & 1 \end{bmatrix} \quad (5)$$

where the spectral radius of  $A$  is equal to  $a$ . We set  $a = 1.8$ ; the system is quite unstable. Nodes 1, 3, 5, 7 receive actuation; the actuation matrix  $B \in \mathbb{R}^{8 \times 4}$  is the  $8 \times 8$  identity matrix  $I$  with columns 2, 4, 6, 8 removed, i.e.

$$\begin{bmatrix} 1 & 0 & 0 & 0 \\ 0 & 0 & 0 & 0 \\ 0 & 1 & 0 & 0 \\ \dots & \dots & \dots & \dots \\ 0 & 0 & 0 & 0 \end{bmatrix} \quad (6)$$

Consider an LQR problem with state penalty  $Q = I$  and no input penalty<sup>1</sup>:

$$\begin{aligned} \min_K \quad & \sum_{t=0}^{\infty} x(t)^\top Q x(t) \\ \text{s.t.} \quad & x(0) = x_0, \quad u(t) = Kx(t) \\ & x(t+1) = Ax(t) + Bu(t) + w(t) \end{aligned} \quad (7)$$

Optimal  $K$  is obtained by solving the DARE. At full actuation (i.e.  $B = I$ ), the optimal  $K$  and the resulting closed-loop responses  $\mathbf{R}$ ,  $\mathbf{M}$  are very sparse; in fact, all are diagonal. However, with the specified actuation matrix (i.e. 50% actuation), sparsity in both the controller and the closed-loop responses are lost, as shown in the ‘‘LQR’’ panels in Fig.

<sup>1</sup>To avoid issues with numerical solvers, we may need to set an input penalty  $R = \epsilon I$  for some  $\epsilon \ll 1$

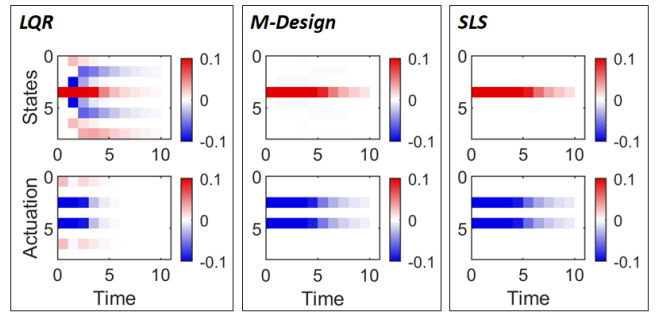


Fig. 2. Impulse responses for the 8-node ring system using the LQR controller, M-Design controller, and SLS controller. At time  $t = 0$ , an impulse disturbance hits node 4. The LQR controller, though optimal, gives a global impulse response; every state and input reacts to this disturbance (the actuation may appear sparse, but this is because only nodes 1, 3, 5, and 7 are actuated). The M-Design and SLS controllers give highly local impulse responses (i.e. highly local closed-loop responses); only nodes 3, 4, and 5 react to this disturbance. Associated normalized costs: 1.000 for LQR, 1.035 for M-Design, and 1.037 for SLS. Despite being highly localized, the M-Design and SLS controllers perform nearly optimally.

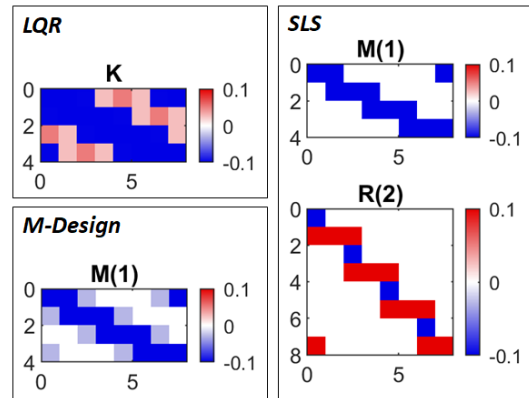


Fig. 3. Sparsity of the LQR controller (implemented using  $K$ ), M-Design controller (implemented using  $M$  and  $R$ ), for the 8-node ring system. All spectral elements  $M(k)$  are constrained to have the same sparsity, so we show  $M(1)$  as a representative element. For  $R$ , all spectral elements are constrained to have the same sparsity except  $R(1)$ , which the SLS feasibility constraint restricts to be the identity matrix; we show  $R(2)$ . The LQR controller is dense, while the other two are constrained to be local. We remark that the SLS controller  $M$  appears to be sparser than the  $M$  matrix from M-Design, even though we applied the same sparsity constraint to both.

3 and Fig. 2). Worse, we are unable to specify any sparsity constraints on the closed-loop responses  $\mathbf{R}$  and  $\mathbf{M}$ , since such constraints would be nonconvex in  $K$  as per Eq. 3. The problem of specifying sparsity on the closed-loop responses in a convex manner is addressed by the SLS parametrization, which we will use in the next section. However, for tutorial purposes, and to introduce the presence of *memory* in our eventual mesocircuit, we will first consider an intermediate parametrization which we call *M-Design*.

### B. M-Design

We want to design a controller and closed-loop responses  $\mathbf{R}$ ,  $\mathbf{M}$  such that all are sparse (i.e. local). However, using the  $\mathbf{u} = \mathbf{K}\mathbf{x}$  state feedback controller makes this problem – particularly, sparsity constraints on  $\mathbf{R}$ ,  $\mathbf{M}$  – highly nonconvex.

Assume that instead of sensing the state  $\mathbf{x}$ , we are able to sense the disturbance  $\mathbf{w}$  directly. Then, we can apply a disturbance feedback controller  $\mathbf{u} = \mathbf{M}\mathbf{w}$ ; this controller works on stable systems and unstable systems with zero initial condition. We emphasize that this is merely a tutorial step; we do not generally expect disturbance sensing to be possible, and we do not expect to use this controller in practice.

Under disturbance feedback,  $\mathbf{M}$  serves as both the controller *and* the closed-loop actuation response. We can now reformulate the original LQR problem from Eq. 7 such that we search over  $\mathbf{M}$  in our optimization instead of  $K$ ; we shall refer to the below as *M-Design*:

$$\begin{aligned} \min_{\mathbf{M}} \quad & \|Q^{\frac{1}{2}}\mathbf{R}\|^2 \\ \text{s.t.} \quad & [zI - A \quad -B] \begin{bmatrix} \mathbf{R} \\ \mathbf{M} \end{bmatrix} = I \\ & \mathbf{R}, \mathbf{M} \text{ stable, causal, } \mathbf{M} \in \mathcal{S} \end{aligned} \quad (8)$$

The first constraint of M-Design ensures that the proposed controller and closed-loop responses obey the original system dynamics. We refer to it as the *feasibility constraint*. In M-Design, we optimize only over  $\mathbf{M}$ , and  $\mathbf{R}$  is determined by  $\mathbf{M}$  via the feasibility constraint. We can additionally constrain  $\mathbf{M}$  to be sparse via the set  $\mathcal{S}$ ; in M-Design, this constraint is affine. Since  $\mathbf{M}$  is both the controller and closed-loop actuation response,  $\mathbf{M} \in \mathcal{S}$  gives sparsity in both the controller and one of the closed-loops. Closed-loop state response  $\mathbf{R}$  is constrained to be stable to ensure overall stability of the system. For now, we will neglect to enforce any sparsity on  $\mathbf{R}$ , though this is also possible in this formulation and gives an affine constraint. In contrast, we could not enforce sparsity on any closed-loop response in the original LQR problem as defined in Eq. 7, as it resulted in nonconvexity.

We now use M-Design to specify 2-hop local sparsity, i.e. each node may only communicate with its neighbors and its neighbor's neighbors. In our ring system, this means each node communicates with two neighbors on each side (e.g. Node 4 communicates with Node 2, 3, 5, 6). The resulting controller and closed-loops are shown in the "M-Design" panels in Fig. 3 and Fig. 2. We see that the desired sparsity is indeed achieved. Also, even though we did not constrain the closed-loop state response  $\mathbf{R}$ , the state impulse response (i.e.  $\mathbf{R}$ ) is highly sparse. Furthermore, the performance of this sparse controller is only 4% worse than that of the optimal, non-sparse controller, despite the drastic difference in sparsity.

In addition to locality-motivated sparsity, the M-Design formulation can also deal with other types of sparsity, i.e. delayed communication in the controller. Delayed communication is common in biological systems; neural signaling is generally orders of magnitude slower than man-made electrical signaling, and slower neurons are often preferred because they are less expensive to maintain [13]. For very large cyber-physical systems (e.g. power grids), delay-tolerant controllers are important as the distances spanned by such systems make

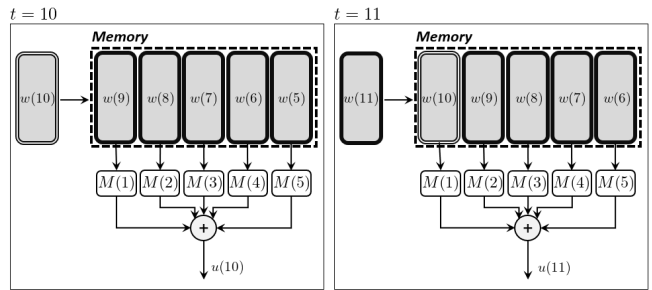


Fig. 4. Standard implementation of a system with FIR transfer function  $\mathbf{M}$ , input  $\mathbf{w}$ , and output  $\mathbf{u}$ . This example uses a strictly causal  $\mathbf{M}$  (i.e.  $M(0) = 0$ ) with horizon length  $T = 5$ . (Left) At time  $t = 10$ ,  $w(t)$  from the  $t = 5$  to  $t = 9$  are in memory. The output  $u(10)$  is produced by summing  $M(k)w(t - k)$  from  $k = 1$  to  $k = 5$ . (Right) At the next timestep,  $t = 11$ , the entries in memory shift to the right. The oldest value,  $w(5)$ , is discarded (i.e. forgotten), and the newest value,  $w(10)$ , enters the memory from the left. The output  $u(11)$  is again produced by summing products of  $M(k)w(t - k)$ .

instant communication impossible. In our companion paper [2], we used standard full control and state feedback to model delays by including extra delay states. We can replicate results therein using M-Design; instead of introducing extra delay states, we merely have to appropriately constrain the sparsity of  $\mathbf{M}$ . Thus, our proposed intermediate formulation (and the final SLS formulation) easily accommodates delays that can be modeled using standard control tools.

### C. Local memory patches

We introduce the notion of a local memory patch using the M-Design controller. Though the M-Design controller is completely comprised of forward pathways, the local memory mechanism will play an important role in the SLS mesocircuit with IFPs in the next section.

First, we write out the controller  $\mathbf{u} = \mathbf{M}\mathbf{w}$  as a time-domain convolution. We assume  $\mathbf{M}$  to have some finite horizon length  $T$ :

$$u(t) = \sum_{k=0}^T M(k)w(t - k) \quad (9)$$

To carry out this computation, we require a memory of the most recent  $T$  values of  $w$ . Every time step, we discard the oldest value of  $w$  from memory and add the newest value of  $w$ . An example of this is shown in Fig. 4. This is a standard implementation of a system with FIR transfer matrix  $\mathbf{M}$ ; we will build upon it to create locally implemented controllers and memory patches. We remark that although increased  $T$  generally improves performance, it requires more memory.

Suppose we solve Eq. 8 with some local sparsity constraints on  $\mathbf{M}$ . We can then implement  $\mathbf{M}$  using some standard realization. This gives the desired sparsity in the closed-loop  $\mathbf{M}$ , but does not necessarily preserve the desired communication sparsity in the controller; i.e. the resulting controller may communicate globally, which we don't want. We now provide a natural controller implementation that preserves sparse communication, and defer exploration of other sparsity-preserving controller realizations to future work.

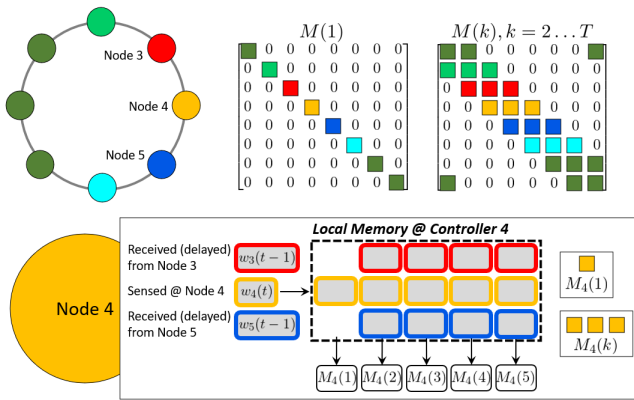


Fig. 5. (Top left) Ring with 8 nodes. (Top right) Spectral elements of  $\mathbf{M}$ , the disturbance feedback controller. Colored squares represent nonzero values; all other values in the matrices are constrained to be zero. Nonzero values away from the diagonal represent communication between nodes. Sparsity constraints come from both delayed communication (as exemplified by  $M(1)$ ) and local communication (as exemplified by  $M(k)$  for  $k > 2$ ). In M-Design,  $\mathbf{M}$  is also the closed-loop actuation response, so sparsity on  $\mathbf{M}$  additionally translates to local disturbance rejection by actuators. (Bottom). Local controller and memory patch at node 4. Each node uses its own rows of  $M(k)$  to implement its own controller locally. Rectangles in local memory represent scalar values of  $w_i(t)$ . Colors on the rectangles correspond to the node that the value came from; red rectangles pertain to  $w_3$  values from node 3, and blue rectangles pertain to  $w_5$  values from node 5. Most recent entries are on the left, and oldest entries are on the right. Local actuation (not shown) is produced by calculating products of  $M_4(k)$  with columns in memory, and summing over these products. Local sparsity constraints in  $\mathbf{M}$  ensures that we only require knowledge and memory of local (i.e. neighboring) elements.

We implement  $\mathbf{M}$  in a distributed way: each node implements its own controller with its own local memory patch. We show an example in Fig. 5, where each node communicates only with its immediate neighbors. We additionally demonstrate the principle of communication delay and its relation to the sparsity of  $M(k)$ ; in our case, we enforce a delay of step 1, such that each node only receives information from its neighbors after one step of delay. The M-Design framework allows for arbitrary sparsity structure on  $\mathbf{M}$ , provided the feasibility constraint can be satisfied.

Since each node has its own local memory, a lot of redundant memory is created. In our example, the memory at node 4 stores past values of  $w_3$ ; past values of  $w_3$  are also stored at node 3 and node 2. Here, each disturbance  $w_i$  is stored thrice: by node  $i$  and its neighbors  $i + 1$  and  $i - 1$ . With increased locality size, the total memory and total repetition is greatly increased. For example, if each node on the ring communicates to the 4 nearest neighbors instead of 2 nearest neighbors, then each disturbance  $w_i$  would be stored 5 times: once by node  $i$ , and once each by its 4 neighbors. For a general system, each disturbance  $w_i$  will be stored by node  $i$  and all neighbors to whom it communicates. This appears to be a fundamental cost of distributed processing: although local memory patches are small relative to the total number of nodes, global memory (i.e. the sum of all local memory patches) is larger than the total number of nodes due to the many duplicate copies.

Fig. 5 shows the local memory patch at only *one* node.

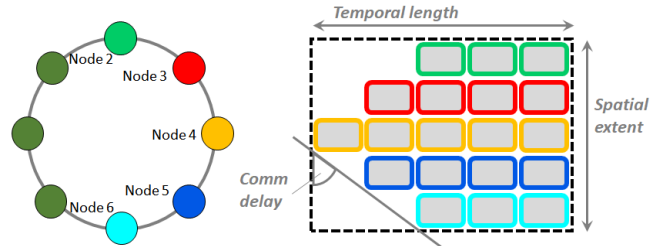


Fig. 6. (Left) Ring with 8 nodes. (Right) Size and shape of example local memory patch at node 4. New information enters on the left, old information exits (i.e. is forgotten) on the right. Temporal length  $T$  indicates how far to remember into the past. Spatial extent indicates how many neighbors each node communicates with. Communication delay is indicated by the angle of the triangular ‘front’ of the memory; a larger angle corresponds to larger delay. In this example,  $T = 5$ , and nodes communicate to their 4 nearest neighbors with delay proportional to distance. In memory, node 4 has up-to-date information on node 4 (in yellow), slightly outdated (delay of one timestep) information on nodes 3 and 5 (in red and blue), and more outdated (delay of 2 timesteps) information on nodes 1 and 6, which are farther away.

A more detailed characterization of each local memory patch is shown in Fig. 6. Note that this triangular shape only holds for ring or chain systems; for more general systems there will be a similar phenomenon where some rows of local memory are shorter than others due to varying communication delay. We can also specify self-delay; e.g. sensor  $i$  communicates to controller  $i$  with some nonzero delay. Additionally, in our example, we assume that the size of the local memory patches are uniform across nodes; however, this need not be the case in general. Different nodes may store local memory patches of varying size. All of this is supported by the M-Design formulation; one must only specify the appropriate sparsity constraint on  $\mathbf{M}$  in Eq. 8.

As with all control systems and transfer functions, there are multiple ways to realize and implement a given controller. Our case is somewhat unique, as we impose implementation-level (e.g. communication) constraints on the controller directly. However, alternative implementations still exist. For instance, instead of an explicit local memory patch, memory may be implicitly carried by delayed wires; e.g. instead of node 4 having  $w_3(t)$ ,  $w_3(t - 1)$ , and  $w_3(t - 2)$  in a local memory patch, there can simply be three wires from node 3 to node 4 with delay of 0, 1, and 2. Nonetheless, the general observations regarding memory length and duplication – which will be important in our next section regarding SLS and IFP – still apply to these alternative implementations. The question of general system realization and implementation with implementation-level constraints is deferred to future work.

### III. MESOCIRCUITS FOR INTERNAL FEEDBACK

We use SLS to produce a ‘mesocircuit’ that predicts large amounts of IFPs relative to forward pathways, purely from *a priori* principles. This prediction is consistent with observations in the brain [4]–[6] and also incorporates local communication, local disturbance rejection, and signaling delay: features that are ubiquitous in the nervous system, as described in the previous section. We make extensive use

of the notions of locality and memory from the M-Design controller.

**Definition 1.** A *mesocircuit* refers to a physiological circuit in an organism. It concerns  $\sim$ thousands (or more) of cells and/or neurons working together to provide some functionality. A mesocircuit is a larger-scale entity than a *microcircuit*, which concerns individual cells and neurons; but a smaller-scale entity than the circuit shown in the left panel of Fig. 1, in which circuit components (e.g. V1 [14]) are composed of  $\sim 10^7$  neurons.

The above definition of a mesocircuit is consistent with terminology in neuroscience literature. In our case, a single ‘node’ in our analysis may correspond to a cluster of cells or neurons in an organism.

### A. System Level Synthesis

In M-Design, we assumed disturbance-sensing capabilities, and implemented a basic disturbance feedback controller. This allowed us to specify sparsity constraints on controller and closed-loop responses in an affine manner. Now, we remove the disturbance-sensing assumption and revert to basic state feedback. As before, we still wish to impose sparsity constraints on the controller and closed-loop responses: we achieve this with System Level Synthesis (SLS) [11]. The SLS formulation of the original LQR problem Eq. 7 is as follows:

$$\begin{aligned} \min_{\mathbf{R}, \mathbf{M}} \quad & \|Q^{\frac{1}{2}} \mathbf{R}\|^2 \\ \text{s.t.} \quad & [zI - A \quad -B] \begin{bmatrix} \mathbf{R} \\ \mathbf{M} \end{bmatrix} = I \\ & \mathbf{R}, \mathbf{M} \text{ stable, strictly causal} \\ & \mathbf{R}, \mathbf{M} \in \mathcal{S} \end{aligned} \quad (10)$$

where the first constraint, the *feasibility constraint*, ensures that the closed-loop responses  $\mathbf{R}, \mathbf{M}$  are feasible. Once we solve this optimization problem, we use  $\mathbf{R}$  and  $\mathbf{M}$  to implement the controller, as shown in Fig. 7. Feasibility, stability, and robustness of this formulation and implementation are discussed at length in [11].

SLS is a natural next step to M-Design. Now, instead of sensing the disturbance, we use IFPs (see Fig. 7) to recreate it. Here, the IFP represents an estimate of the state based on past sensed states  $x$  and our own previous actions  $u$ . We subtract this from the true sensed state to produce an estimate of the disturbance. This disturbance is used to generate the control output via  $\hat{\mathbf{M}}$ ; it is also used to generate the state estimate via  $\hat{\mathbf{R}}$ .

In M-Design, we use  $\mathbf{M}$  as both the controller and closed-loop response; in SLS, both  $\mathbf{R}$  and  $\mathbf{M}$  are controller and closed-loop response. The feedback structure used to implement the controller ensures that sparsity in  $\mathbf{R}$  and  $\mathbf{M}$  translate directly to sparsity on the controller. Additionally, the feasibility constraint ensures that by using the controller from Fig. 7, the closed-loop responses of the system also become  $\mathbf{R}$  and  $\mathbf{M}$ , as per Eq. 2 (see Thm 4.1 in [11]).

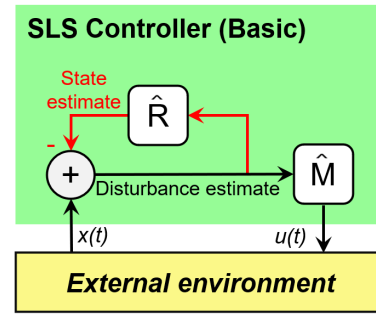


Fig. 7. Block diagram for state feedback SLS controller.  $\hat{\mathbf{R}}$  is equivalent to  $z\mathbf{R} - I$ , and  $\hat{\mathbf{M}}$  is equivalent to  $z\mathbf{M}$ . Any sparsity in  $\mathbf{R}$  and  $\mathbf{M}$  directly translate to sparsity in the controller. The IFP (in red) with  $\hat{\mathbf{R}}$  takes the disturbance estimate and produces a state estimate; this is then subtracted from the true state to produce the disturbance estimate. Note: since SLS constrains  $\mathbf{R}, \mathbf{M}$  to be strictly causal,  $\hat{\mathbf{R}}$  and  $\hat{\mathbf{M}}$  are causal.

Similar to M-Design, we can enforce sparsity constraints on  $\mathbf{R}, \mathbf{M}$  via  $\mathcal{S}$ ; these become affine constraints in the Eq. 10. We use SLS to design a controller for the 8-node ring that is localized in both controller and closed-loop response, shown in the ‘‘SLS’’ panels of 3 and 2. As with the M-Design case, the performance of this sparse controller is less than 4% worse than that of the optimal, non-sparse controller.

We remark that by specifying constraints on  $\mathbf{R}, \mathbf{M}$ , we automatically constrain both the controller and closed-loop. In our example, we use this to our advantage; however, there are cases where we don’t want to constrain both. In such cases, we may use an adjusted version of Eq. 10 [15], [16]. For our ring system, we can additionally incorporate communication delay constraints as described in Fig. 6. In this case, the delay-motivated sparsity constraints are excessive for the closed-loop and render the optimization in Eq. 10 infeasible. We instead use the ‘virtually localized’ SLS formulation described in [15]. This yields a controller that is locally implemented and communicates with delay, but imposes no constraints on the closed-loop response. The resulting impulse response and controller sparsities are shown in Fig. 8. Though the extremely delayed and sparse controller is able stabilize the system, the total cost is roughly double that of the optimal unconstrained LQR controller; this delay constraint is very harsh, especially since the system is highly unstable. The ‘virtually localized’ SLS formulation in question, as well as the methods presented in [16], utilize the same controller structure as standard SLS, shown in Fig. 7. Thus, the resulting controller structure remains unchanged, and the discussion on memory, mesocircuits, etc. still apply to these SLS-based methods.

We now present the full SLS mesocircuit at a single node, in Fig. 9. In the full circuit, instead of communicating sensed disturbances  $w$  (as we did in M-Design), we communicate estimated disturbances  $\hat{\delta}$  (note: this is a time-shifted estimate, e.g.  $\hat{\delta}(t)$  is the estimate for  $w(t - 1)$ ). The memory is processed by  $\mathbf{M}$  to produce an output  $u$ ; the memory is also processed by  $\mathbf{R}$  to produce the estimated disturbance  $\hat{\delta}$ . The path through  $\mathbf{R}$  is clearly an IFP, and coincides with prevailing notions of IFPs as predictive functionality [5],

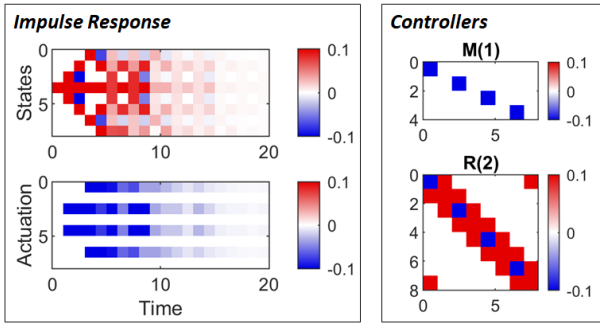


Fig. 8. Impulse response and controller sparsity for the 8-node ring system using the ‘virtually localized’ SLS controller with both local and delayed communication constraints. Compared to the controllers that produced Fig. 2, this controller incorporates additional communication delay constraints, as described in Fig. 6. Note the extreme sparsity of  $M(1)$  (subsequent spectral elements have sparsity identical to  $M(1)$  of Fig. 3). The associated normalized cost compared to standard LQR is 2.101; the added communication delay represents a harsh constraint, especially for this unstable plant.

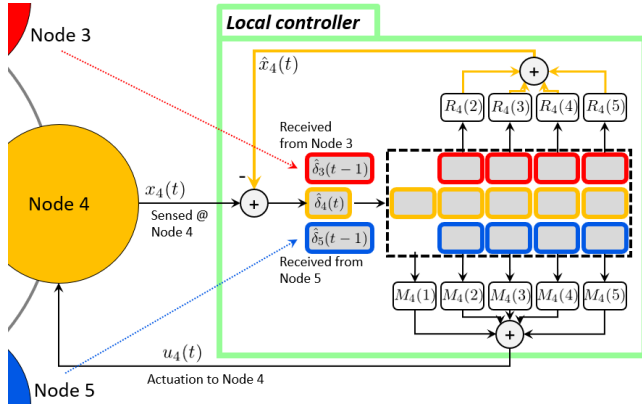


Fig. 9. Local SLS controller (mesocircuit and memory) at node 4. Memory is used by both the forward path (through  $\mathbf{M}$ ) and IFP (through  $\mathbf{R}$ ). We enforce inter-node communication delay;  $\hat{\delta}_3$  and  $\hat{\delta}_5$  are received from neighboring nodes with a delay of 1 timestep. Note that  $R(1)$  is not included because for all  $\mathbf{R}$  satisfying the feasibility constraint in Eq. 10, the IFP expression  $z\mathbf{R} - I$  (see Fig. 7) results in  $R(1)$  being canceled out.

[17]. The memory patch itself is part of both the forward path and and IFP. All that remains now is for us to show how this mesocircuit predicts IFPs that greatly outnumber forward paths.

### B. Full Mesocircuit

We show three local SLS mesocircuits in Fig. 10. Here, node 4 has no actuation, but still requires memory and circuitry to calculate its local estimated disturbance  $\hat{\delta}_4$  and communicate to its neighbors. The actuated nodes have roughly equal parts forward paths and IFP, while the unactuated node has *only* IFP. For our example 8-node ring with 50% actuation, this means that 4 nodes will have equal parts forward paths and IFP, while the other 4 will have purely IFP; in total, we have twice as many IFPs as forward paths, and massive amounts of memory serving both directions. Additionally, as indicated by the dotted colored arrows, subsystems must communicate to one another; these translate to lateral connections, which are often also classified as IFPs

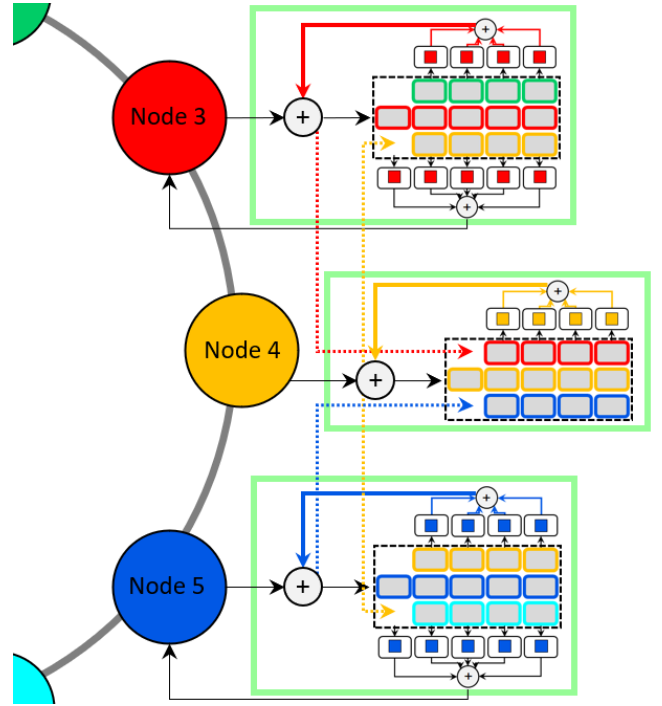


Fig. 10. Local SLS controllers (mesocircuit and memory) at nodes 3, 4, and 5. Each local controller is encircled by a light green box. Only nodes 3 and 5 are actuated. All circuitry at node 4 is purely IFP; though node 4 does not calculate actuation, it must calculate its local estimated disturbance  $\hat{\delta}_4$  and communicate this (via dotted yellow arrow) to its neighbors for use in their calculations. Thus, nodes with actuation have memory, and roughly equal parts forward paths and IFP, while nodes without actuation have memory and pure IFP. For systems in which sensing is much denser than actuation (e.g. nervous system, biological systems), this SLS mesocircuit directly predicts a massive amount of memory and IFP (compared to forward paths).

in neuroscience literature.

For systems with sparser actuation, the amount of IFPs relative to the amount of forward paths becomes even greater. Biological systems, i.e. organisms, sense far more information than they are able to act upon. For instance, we may be able to see things hundreds or thousands of meters into the distance, but we can only act on objects within a small radius around our bodies (and even then, in a manner highly limited by our anatomy, mobility, and strength). Thus, for such highly underactuated systems, our SLS mesocircuit predicts a very large amount of IFPs relative to forward connections, consistent with experimental observations. IFPs in SLS are fundamentally predictive; thus, the large amount of IFPs suggests that to achieve good performance in a distributed, underactuated system, we must predict more than we can act on. Overall, localized and distributed processing are the main features that motivate IFPs in our mesocircuit. These features are not captured in standard models involving IFPs – indeed, prior to SLS, no optimal controller model *could* capture localized and distributed processing. Although other models (e.g. modulation and memory processes, gain control, [5] predictive coding [17], recurrent neural networks [18], Bayesian estimation [2]) contain IFPs, our model produces the largest amount of IFPs. In our model, IFPs are not merely

supplements to the forward processing path, but are crucial to function of the overall system.

We remark that we have focused on the standard implementation of the distributed state feedback SLS controller in order to create this mesocircuit. This controller is internally stable [11] and is applicable to any system. Other SLS controllers, namely full control and output feedback, also contain IFPs. Alternate state feedback realizations and implementations are discussed in [19], [20]; both preserve the central IFP feature, though they are focused more on distributed implementation than *localized* implementation. [20] discusses controllers that reducing requisite memory, though the proposed controllers are only for open-loop stable plants with some non-local communication between nodes; our implementation works on any plant and requires only local communication. In general, there are likely additional steps that can be employed to simplify our mesocircuit; however, we anticipate that the general observation regarding the amount of IFPs relative to the amount of forward paths will hold. We defer an exploration of implementation details to future work; such details may be best suited for iteration with experimental results; candidate systems are described in our companion paper [1]. Additionally, we desire comprehensive theory regarding sparsity-preserving controllers; this is the subject of future work, and aims to unite SLS-based IFPs and delay-state-based IFPs of the form described in our companion paper [2], as well as other sources of IFP.

In addition to forming the basis for this mesocircuit, SLS also enjoys unique scalability benefits, which we anticipate to be useful when producing large-scale models using SLS.

#### IV. CONCLUSION

We presented an SLS-based mesocircuit for sensorimotor modeling. From *a priori* principles of local processing, local disturbance rejection, and underactuation, our mesocircuit predicts a high ratio of internal feedback pathways (IFPs) to forward pathways. This has striking resemblance to observations in neuroanatomy; our model complements data-driven techniques in neuroscience and provides human-interpretable ideas on the function of IFPs in the nervous system. Future work will aim to incorporate more neuronal features (e.g. noise) and produce more realistic sensorimotor models that can more quantitatively connect to experiments in neuroscience. We also plan to use this mesocircuit to model biological systems, in collaboration with neuroscientists and biologists; potential experiments and systems of interest are discussed in our companion work [1].

#### REFERENCES

[1] A. A. Sarma, J. S. Li, J. Stenberg, G. Card, E. S. Heckscher, N. Kasthuri, T. Sejnowski, and J. C. Doyle, "Internal feedback in biological control: Architectures and examples," 2021. [Online]. Available: <https://arxiv.org/abs/2110.05029>

[2] J. Stenberg, J. S. Li, A. A. Sarma, and J. C. Doyle, "Internal feedback in biological control: Diversity, delays, and standard theory," 2021. [Online]. Available: <http://arxiv.org/abs/2109.11752>

[3] D. J. Felleman and D. C. Van Essen, "Distributed hierarchical processing in the primate cerebral cortex," *Cerebral Cortex*, vol. 1, no. 1, pp. 1–47, 1991.

[4] E. M. Callaway, "Feedforward, feedback and inhibitory connections in primate visual cortex," *Neural Networks*, vol. 17, no. 5-6, pp. 625–632, 2004.

[5] L. Muckli and L. S. Petro, "Network interactions: non-geniculate input to V1," *Current Opinion in Neurobiology*, vol. 23, no. 2, pp. 195–201, 2013.

[6] J. M. Budd, "Extrastriate feedback to primary visual cortex in primates: A quantitative analysis of connectivity," *Proceedings of the Royal Society B: Biological Sciences*, no. 1400, pp. 1037–1044, 1998.

[7] C. Stringer, M. Pachitariu, N. Steinmetz, C. B. Reddy, M. Carandini, and K. D. Harris, "Spontaneous behaviors drive multidimensional, brainwide activity," *Science*, vol. 364, 2019.

[8] S. Musall, M. T. Kaufman, A. L. Juavinett, S. Gluf, and A. K. Churchland, "Single-trial neural dynamics are dominated by richly varied movements," *Nature Neuroscience*, vol. 22, no. 10, pp. 1677–1686, 2019.

[9] E. Todorov, "Optimality principles in sensorimotor control," *Nature Neuroscience*, vol. 7, no. 9, pp. 907–915, 2004.

[10] D. W. Franklin and D. M. Wolpert, "Computational mechanisms of sensorimotor control," *Neuron*, vol. 72, no. 3, pp. 425–442, 2011.

[11] J. Anderson, J. C. Doyle, S. H. Low, and N. Matni, "System level synthesis," *Annual Reviews in Control*, vol. 47, pp. 364–393, 2019.

[12] N. Suga, "Role of corticofugal feedback in hearing," *Journal of Comparative Physiology A: Neuroethology, Sensory, Neural, and Behavioral Physiology*, vol. 194, no. 2, pp. 169–183, 2008.

[13] P. Sterling and S. B. Laughlin, *Principles of neural design*. MIT Press, 2015.

[14] M. Colonnier and J. O’Kusky, "Number of neurons and synapses in the visual cortex of different species," *Revue canadienne de biologie*, vol. 40, no. 1, pp. 91–99, Mar 1981.

[15] N. Matni, Y. S. Wang, and J. Anderson, "Scalable system level synthesis for virtually localizable systems," in *IEEE Conference on Decision and Control*, 2017, pp. 3473–3480.

[16] J. S. Li and D. Ho, "Separating controller design from closed-loop design: A new perspective on system-level controller synthesis," in *IEEE American Control Conference*, 2020, pp. 3529–3534.

[17] Y. Huang and R. P. Rao, "Predictive coding," *Wiley Interdisciplinary Reviews: Cognitive Science*, vol. 2, no. 5, pp. 580–593, 2011.

[18] A. Nayeibi, D. Bear, J. Kubitius, K. Kar, S. Ganguli, D. Sussillo, J. J. DiCarlo, and D. L. Yamins, "Task-driven convolutional recurrent models of the visual system," in *NeurIPS*, 2018, pp. 5295–5306.

[19] J. Anderson and N. Matni, "Structured state space realizations for SLS distributed controllers," in *IEEE 55th Annual Allerton Conference on Communication, Control, and Computing*, no. 2, 2017, pp. 982–987.

[20] S.-H. Tseng and J. Anderson, "Deployment Architectures for Cyber-Physical Control Systems," in *IEEE American Control Conference*, 2020, pp. 5287–5294.